IOPscience iopscience.iop.org

Home Search Collections Journals About Contact us My IOPscience

Dynamical effects and ergodicity in the dipolar glass phase: evidence from time-domain EPR and phase memory time studies of AsO_4^{4-} in $Rb_{1-x}(NH_4)_xH_2PO_4$ (x = 0,0.5,1)

This article has been downloaded from IOPscience. Please scroll down to see the full text article.

2006 J. Phys.: Condens. Matter 18 4265

(http://iopscience.iop.org/0953-8984/18/17/014)

View the table of contents for this issue, or go to the journal homepage for more

Download details:
IP Address: 129.252.86.83
The article was downloaded on 28/05/2010 at 10:24

Please note that terms and conditions apply.

INSTITUTE OF PHYSICS PUBLISHING JOURNAL OF PHYSICS: CONDENSED MATTER

J. Phys.: Condens. Matter **18** (2006) 4265–4284 doi:10.1088/0953-8984/18/17/014

Dynamical effects and ergodicity in the dipolar glass phase: evidence from time-domain EPR and phase memory time studies of AsO_4^{4-} in $Rb_{1-x}(NH_4)_xH_2PO_4$ ($x = 0, 0.5, 1$)

M D Sastry[1,4], H Gustafsson[2], M Danilczuk[1,3] and A Lund[1]

[1] Department of Physics and Measurement Technology, Linköping University, S-581 83 Linköping, Sweden
[2] Department of Medicine and Care, Radiation Physics, Faculty of Health Sciences, Linköping University, S-581 85 Linköping, Sweden
[3] Institute of Nuclear Chemistry and Technology, Dorodna 16, 03-195 Warsaw, Poland

E-mail: mdsastry@yahoo.co.in, hakgu@imv.liu.se, marda@ifm.liu.se and alund@ifm.liu.se

Received 26 December 2005, in final form 10 March 2006
Published 13 April 2006
Online at stacks.iop.org/JPhysCM/18/4265

Abstract

Three-pulse electron spin echo envelope modulation (ESEEM), hyperfine sublevel correlation spectroscopy (HYSCORE) investigations and two-pulse electron spin echo (ESE) measurements of phase memory time T_M, were carried out, in the 20–200 K temperature range, on an AsO_4^{4-} paramagnetic probe stabilized in RbH_2PO_4 (RDP), $NH_4H_2PO_4$ (ADP), and dipolar glass $Rb_{0.5}(NH_4)_{0.5}H_2PO_4$ (RADP). The results obtained on ADP revealed hyperfine interaction of the probe ion with the ^{14}N of the ammonium ion, the coupling constant satisfying the condition of 'cancellation' at a field of 480 mT. The ammonium ion was found to be in two different sites in ADP, which became indistinguishable on the formation of dipolar glass RADP. These results were confirmed by HYSCORE spectral measurements. The fast Fourier transform (FFT) spectra of three-pulse ESEEM decays have clearly revealed the interaction with protons in the O–H$\cdots$O bond both in ADP and RDP; and in RADP with an averaged coupling constant. The phase memory times in RADP exhibited strong temperature dependence and were found to be dependent on the nuclear spin quantum number m_I of ^{75}As. The temperature dependence of T_M exhibited a well-defined maximum around 90 K, coinciding with the temperature of onset of 'freezing' in $Rb_{0.5}(NH_4)_{0.5}H_2PO_4$. This is symptomatic of dynamic fluctuations in the dipolar glass phase, with onset around 150 K, going through a maximum around 90 K and slowing down on further cooling. These results suggest that in RADP, a dynamical mechanism with progressive slowing down below 90 K is operative in the glass formation. This implies that the RADP system, with $x = 0.5$, exists in an ergodic relaxor (R)-state in the

[4] Present address: Physical Research Laboratory, Navrangpura, Ahmedabad 380 009, India.

 © 2006 IOP Publishing Ltd Printed in the UK

20–200 K temperature range wherein every fluctuating monodomain can be viewed as statistically representative of the whole sample.

(Some figures in this article are in colour only in the electronic version)

1. Introduction

The dynamic and static properties of systems in which randomly competing interactions result in the formation of a glassy state at low temperatures have attracted considerable attention in the recent past [1]. Magnetic systems with random competing interactions exhibiting the spin glass state [2], mixed ABO_3 type 'relaxor' ferroelectrics and mixed crystals of rubidium dihydrogen phosphate (RDP) and ammonium dihydrogen phosphate (ADP), $Rb_{1-x}(NH_4)_xPO_4$ (RADP) where x is the fractional content of ammonium ion, in the range $0.2 \leqslant x \leqslant 0.73$, termed a dipolar glass, come in this important category of disordered systems [3, 4]. The central theme in these investigations has been the elucidation of new physics and the nature of the equilibrium that sets in when two or more competing interactions, inherently of opposite nature, are operative in a system. It is important to know whether the freezing of 'spins' or clusters of spins into a random orientation is a local nonequilibrium dynamic process or a real equilibrium phase transition with an infinite correlation length below a well-defined critical temperature. The first report of the formation of a dipolar glass in hydrogen-bonded ferroelectrics was by Courtens [4, 5]; the phase diagram of the glass formation and other aspects were discussed in detail by Courtens [6]. Among the important and established findings on RADP are: (i) the motion of NH_4^+ freezes in the glassy phase at temperatures much higher than the freezing temperature of the proton system in the O–H$\cdots$O network and the ammonium ion dynamics has no direct relation to glass formation [7, 8]; (ii) the pressure dependence of the dynamic glass transition temperature, T_m, of RADP($x = 0.5$) by Samara [9] led to the important finding that $\mathrm{d}T_m/\mathrm{d}P$ is finite as $T_m \to 0$, which revealed the nonequilibrium nature of the glass transition in RADP. The static freezing temperature, T_0, of the RADP-glass is yet to be determined; and as suggested by Samara [1] the pressure dependence studies may have to be extended over a larger frequency range to get T_0, the true transition temperature to another equilibrium state. The temperature T_0 can be viewed as defining a transition from an ergodic R-state, i.e. a state where every fluctuating nanodomain can be viewed as statistically representative of the whole sample, to a non-ergodic state. These dielectric studies show that the RADP system for $0.2 \leqslant x \leqslant 0.7$ is in a nonequilibrium ergodic state, in the temperature regions so far investigated, in which local clusters/nanodomains do reflect the statistical behaviour of the whole sample.

EPR and ENDOR measurements have been reported extensively [10–20] over the last three decades for elucidation of phase transitions in the KH_2PO_4 (KDP) type of hydrogen bonded ferroelectrics (FEs) and the antiferroelectric (AFE) $NH_4H_2PO_4$. The orientation of hydrogen bonds linking PO_4 tetrahedra plays the central role in the type of ordering that occurs at the transition temperature. In KDP and RDP the 'up–down' ordering of acid protons leads to the FE transition, whereas the 'lateral' proton ordering in ADP results in an antiferroelectric phase. In ADP the hydrogen bond links every nitrogen with four oxygens of neighbouring PO_4 groups forming nearly flat tetrahedra. The change in proton super-hyperfine structure from quintet to triplet in the EPR of AsO_4^{4-} has contributed significantly to the understanding of the phase transition mechanism. Whereas PO_4 sees four equivalent protons in the paraelectric phase it sees two 'close' and two 'distant' protons in the electrically ordered phase; the z principal axis for this interaction will be along the crystallographic c axis (due to up–down

ordering) in RDP whereas it will be perpendicular to the c axis in the case of ADP, due to lateral O–H$\cdots$O ordering. In most of these studies, the radiation induced paramagnetic defect AsO_4^{4-} ion located at PO_4^{3-} site has been effectively used to monitor the proton dynamics in O–H$\cdots$O bonds. Similar studies for understanding the nature of glass formation in RADP have also been reported [21–25]. From the observation that the hyperfine coupling constant of ^{75}As in RADP scaled as the weighted average, for different values of x, of the respective contributions from RDP and ADP, Babu *et al* [21, 23] have suggested that the system fluctuates between ferroelectric (FE) and antiferroelectric (AFE) phases and slowing down of this eventually leads to glassy behaviour in the low temperature range. Dalal and co-workers [22, 24, 25], on the other hand, modelled it as a predominantly static situation in which the signal observed in RADP is the resultant of a statistical average of hyperfine splittings over the various possible near neighbour interactions with little contribution from motional narrowing or the exchange process. In this model the line broadening is essentially inhomogeneous and the line shift is only apparent by the local predominance of rubidium and/or ammonium ions and the signal of RADP composing of two distinct components represents a local antiferroelectric and ferroelectric state of the AsO_4^{4-} unit. In a larger context of understanding the nature of the dipolar glass phase of RADP, the dynamic model suggested by Babu *et al* [21, 23] is consistent with the ergodic relaxor (R) state of RADP, whereas the statistical model [25] in which near neighbour interactions around the probe are governed by statistical variation in the number of ammonium/rubidium ions implies that RADP exists in a non-ergodic state, and the measurable parameters in RADP essentially give the spread in the distribution of individual sites. The issues underlying these contrasting interpretations can possibly be clarified by making hyperfine interaction measurements on an AsO_4^{4-} probe with higher resolution which makes a clear distinction of FE and AFE phases, and also by getting information on factors causing homogeneous broadening of EPR lines and the temperature dependence thereof. With a view to addressing these aspects, the present work is focused on time domain EPR measurements on AsO_4^{4-} stabilized in RDP, ADP and RADP ($x = 0.5$) in the 20–200 K temperature range. Except for a brief report [26], no detailed electron spin echo (ESE) or ESEEM studies on this interesting class of materials are found in the literature.

Electron spin echo (ESE) decay and ESEEM measurements are normally carried out using either two-pulse or three-pulse excitations. In the two-pulse ESE mode the frequency spectrum gets complicated due to the presence of not only basic frequencies but also the harmonics and combination lines. However, its decay is characterized by the phase memory time T_M, and it can be conveniently used to get the information on this parameter [27, 28]. The short phase memory time limitations associated with two-pulse experiments are largely obviated in the case of the three-pulse experiment and the Fourier transform of a three-pulse ESE decay would contain a much simpler (ENDOR-like) frequency spectrum. In three-pulse ESEEM, combination lines can only arise from the evolution of multiple quantum nuclear coherence since electron spins are in a definite state during the evolution period of length T [27], and the combinations of frequencies within the same electron spin manifold are possible.

This work specifically deals with three-pulse electron spin echo envelope modulation (ESEEM), its Fourier transform (FT) spectrum and hyperfine sublevel correlation (HYSCORE) spectra in the low frequency range. Furthermore, measurements of the phase memory time T_M, reflecting the purely homogeneous contribution to the line width, were also carried out and its temperature dependence was investigated in all the three compounds. These measurements have given new structural information on the ammonium ion in ADP and RADP in addition to giving evidence of the onset of fluctuations in RADP below 150 K and their slowing down below 90 K, the temperature of onset of freezing as given by Courtens' phase diagram [6]. Furthermore, the FT of three-pulse ESEEM has given hyperfine structure due to protons clearly

distinguishable in FE and AFE phases, with the corresponding signal in $x = 0.5$ RADP occurring midway between them. All these results are consistent with a dynamical model, in which the system undergoes a dynamic fluctuation between FE and AFE phases, which in turn suggests the existence of RADP in the ergodic R-state in the 20–150 K temperature range.

2. Experimental details

Ammonium dihydrogen phosphate was obtained from Johnson Matthey GmbH and rubidium dihydrogen phosphate was prepared by reacting rubidium carbonate with orthophosphoric acid and purified by repeated crystallization. RADP was prepared from an appropriate mixture of ADP and RDP. In all the three matrices 0.5 mol% of ammonium dihydrogen arsenate was added as an impurity, and the samples were x-irradiated typically to a dose of 1.6 kGy at room temperature. Single crystals of all the three matrices were grown by slow evaporation, and the orthorhombic crystals obtained had parallelepiped shape with well-defined crystallographic c-axis. No attempts were made to determine the arsenate content by chemical analysis. The intensities of CW-EPR signals in the respective matrices and their temperature dependence would not be same in all matrices in view of large differences in dielectric constants and the corresponding changes in the Q of the loaded cavity. Some of these aspects were given in an earlier publication [21] by one of the authors and his colleagues.

The pulse EPR experiments were conducted using a Bruker Elexys 580 FT/CW X-band spectrometer equipped with a Bruker EN4118X-MD4-W1 dielectric resonator and Bruker Elexys software. The two-pulse sequence used was $\pi/2$–τ–π–τ-echo in which τ was varied to follow the decay of the electron spin echo. The three-pulse ESEEM experiments were conducted using the pulse sequence $\pi/2$–T–$\pi/2$–τ–$\pi/2$–T-echo (stimulated echo). In this pulse sequence τ was incremented in steps of 4 ns and the value of T was kept constant at 200, 248 or 300 ns. The $\pi/2$ pulse width was 16 ns in both two- and three-pulse experiments. The phase memory time was measured using an ordinary two-pulse sequence ($\pi/2$–τ–π–τ-echo) with $\tau = 184, 188, 192, \ldots$ ns. The echo intensity was plotted as a function of τ and was approximated as a single exponential decay. The Bruker Xepr software was used to fit the function $y = A\exp(-\tau/T_{\mathrm{M}})$ to the decay profile of the echo. The modulation amplitude was small compared to the echo intensity; therefore it did not cause any problem during the fit. The temperature dependence of T_{M} was investigated by measuring T_{M} at different temperatures and the spread in T_{M} was estimated from the values obtained during heating and cooling cycles. The FFTs of the three-pulse ESEEM patterns were obtained after zero filling the background corrected modulation pattern. Some 2D four-pulse experiments were conducted with the standard pulse sequence $\pi/2$–τ–$\pi/2$–t_1–π–t_2–$\pi/2$–τ-echo with $\tau = 200$, 248 and 300 ns. The data were processed by standard Bruker software to obtain hyperfine sublevel correlation spectroscopy (HYSCORE) information. The temperature variation studies between room temperature and 10 K were conducted using an Oxford cryogenic system, with liquid helium as the refrigerant. The temperature stability was found to be ± 2 K during this experiment.

3. Results

In view of the different types of measurements carried out, the essential conclusions pertaining to the specific measurement are summarized together with the experimental results in each subsection below and they are used subsequently in section 4 to present a holistic picture.

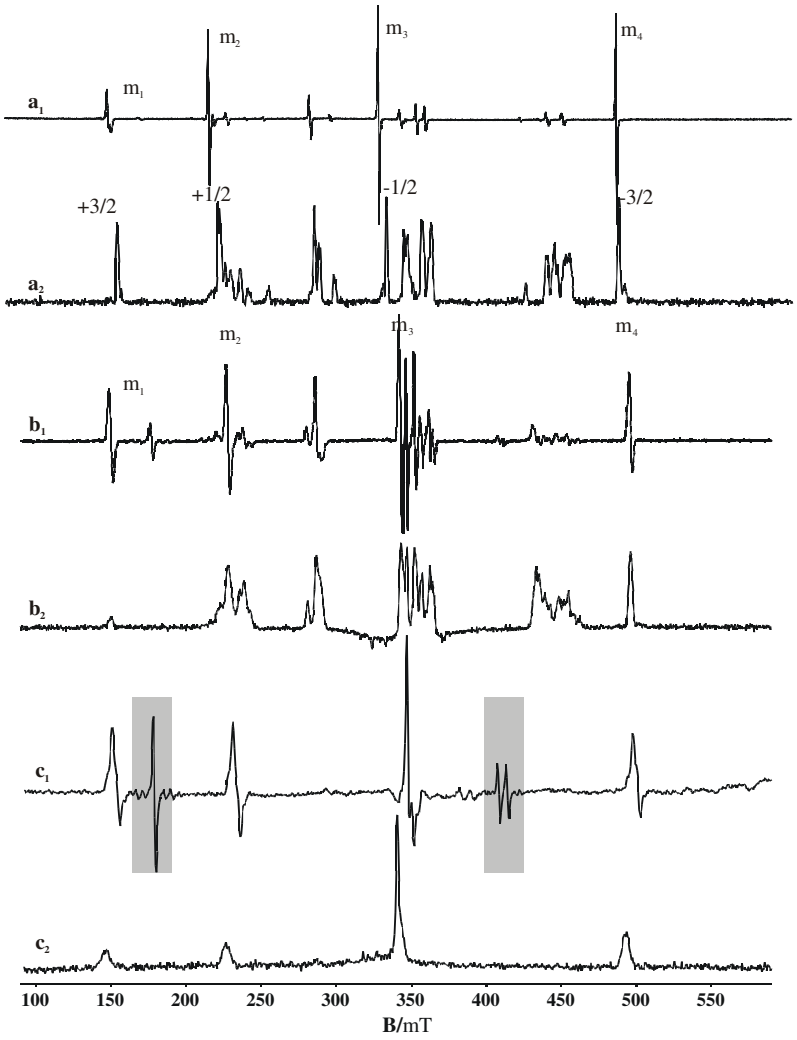

Figure 1. CW-EPR and the corresponding field swept spin echoes for ADP (a_1, a_2) RADP (b_1, b_2) and RDP (c_1, c_2). The crystal orientation is ∼5° from the *c*-axis in the *ac* plane. The EPR spectra and the echoes were recorded at 40 K. The lines marked m_1-m_4 are due to the main radical AsO_4^{4-}. The other lines observed clearly in ADP and RADP are due to the minority radical AsO_3^{2-}. The lines in the shaded areas (c_1) are due to some contamination in the cavity. The differences in the line positions of CW-EPR and field swept echo spectra for ADP are due to a slight mismatch between the respective traces.

3.1. CW-EPR and field swept echo

The CW-EPR spectra of the AsO_4^{4-} centres in the lattices studied have been discussed by a number of workers previously. The spectra obtained in the present work are essentially similar to those reported earlier [14]. Figure 1 shows a typical CW-EPR and the corresponding field swept echoes obtained for the AsO_4^{4-} radical in ADP, RADP and RDP at 40 K, for the external magnetic field a few degrees off from the *c*-axis in the *ac* plane. Lines marked m_1–m_4 are due to the main AsO_4^{4-} radical giving rise to hyperfine interaction with ^{75}As ($I = 3/2$).

The appearance of impurity resonances, marked in figure 1, seems to be due to random contamination, as those signals were observed during some other measurements also. This problem was more obvious in the case of RDP. Some shift in the line position of m_3 in the field swept echo compared to CW-EPR was seen in the case of ADP. It appears that it is partly due to slight mismatch in the line positions in the CW-EPR and field swept echo traces. A slight disturbance in the crystal orientation during the experiment could also have caused a relative shift in the position of m_3. During T_M measurements, in each case the echo was optimized for individual lines. So, the misalignment did not contribute any measurement of importance. The relative intensities in the field swept echo and those in EPR are quite different. The intensity in the field swept echo depends upon the relaxation times of the respective radical ions. In ADP and RADP, in addition to the main AsO_4^{4-}, spectra due to some minority radicals assigned to AsO_3^{2-} were also present. These are shown in figure 1. The field swept echo of the minority radical in ADP and RADP was observable even at room temperature. In order not to digress from the aspects under investigation, a study of the minority radicals will not be presented here. The highest and lowest field lines of the radical under investigation, namely AsO_4^{4-}, are quite free from interference from other radicals, and the ESEEM results obtained on these two lines are presented below, as they give additional advantage in the proper assignments, due to the difference in their resonance fields by nearly a factor of three.

3.2. Three-pulse ESEEM and frequency spectra

The three-pulse stimulated echoes were used to get the ENDOR-like hyperfine interaction information of ^{1}H, ^{14}N, ^{31}P, and ^{85}Rb, interacting with AsO_4^{4-} in the ADP, RDP and RADP lattices. At cancellation conditions, where ESEEM frequencies correspond to nuclear quadrupole resonance (NQR) frequencies, highly resolved spectra could be obtained [29–31] from ^{14}N couplings even in orientationally disordered systems. In order to confirm this and also to obtain clearer information, wherever possible, three-pulse ESEEM measurements were also made on powdered samples of ADP, RADP and RDP. These experiments have given some helpful information, and will be presented below after presenting the results on the respective single-crystal samples.

3.2.1. Ammonium dihydrogen phosphate (ADP) single crystal. The three-pulse spin echo measurements were carried out by locking the field on the low field line (161.1 mT) and the high field line (480.3 mT) of the AsO_4^{4-} centre. The frequency domain spectra obtained at 40 K are shown in figures 2(a) and (b), respectively. For ^{14}N ($I = 1$) with substantial nuclear quadrupole interaction, six ESEEM signals are expected, three in each M_S manifold; two of them correspond to single quantum transitions whereas the third is related to a double quantum transition [31]. However, at the exact cancellation condition, namely, $A_{iso} = 2\nu_N$, the ESEEM frequencies for one electron spin manifold correspond to the NQR frequencies and exhibit no orientation dependence. The FT of the three-pulse ESEEM, at a magnetic field of 480.3 mT, revealed a typical NQR-like pattern of ^{14}N in the 0–5 MHz range [29, 31]. The absence of these features in the ESEEM at the static field of 161.1 mT is consistent with the applicability of the cancellation condition at 480.3 mT and the identification of ^{14}N quadrupole split lines. At a static field of 480.3 mT, the Larmor frequency of ^{14}N is 1.48 MHz. The cancellation condition in first approximation implies $A_{iso} = 2.96$ MHz, but it might be satisfied even under the less rigorous criterion $|A_{iso} - 2\nu_N| < e^2qQ/3h$. When the echo of the low field (161.1 mT) transition is monitored, $A_{iso} > 2\nu_N$ (=0.99 MHz), and the pure quadrupole split lines at low frequencies are not expected to be seen. There would be six lines per site of the ammonium ion, all of them appearing in the low frequency range. The experimental observation shown in

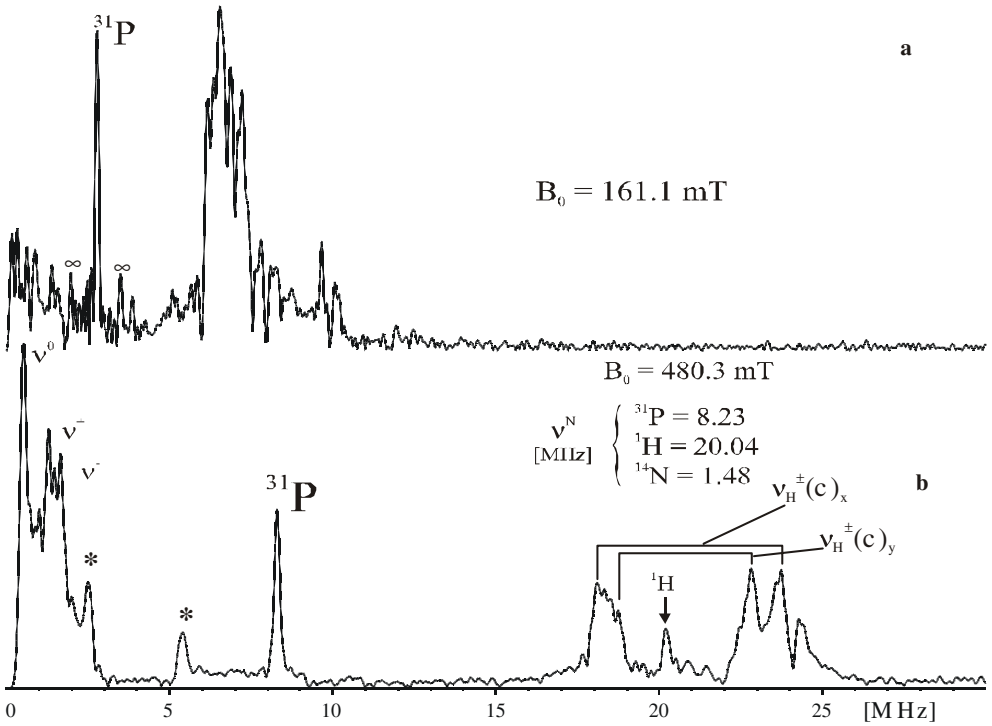

Figure 2. FT of three-pulse ESEEM of AsO_4^{4-} in ADP. (a) Low field ($m_I = +3/2$) hyperfine component and (b) high field ($m_I = -3/2$) At high field the cancellation condition is satisfied for the ^{14}N nucleus (see the text). The static magnetic field makes ∼5° with the *c*-axis in the *ac* plane. The lines marked (*) at low frequency are assigned to combination quadrupolar lines involving ^{14}N. The high frequency lines are due to ^{1}H couplings of close protons. The satellites in the close vicinity of ν_H (free) are due to distant protons.

figure 2(a) is in agreement with this possibility. The NQR-like quadrupole frequencies under the cancellation condition, in the standard notation, are given by the equations

$$\nu_0 = \frac{e^2qQ}{2h} \cdot \eta \tag{1a}$$

$$\nu_- = \frac{e^2qQ}{4h} \cdot (3 - \eta) \tag{1b}$$

$$\nu_+ = \frac{e^2qQ}{4h} \cdot (3 + \eta). \tag{1c}$$

The peaks around 1–1.25 MHz and 1.75–2.0 MHz are assigned to ν_- and ν_+ respectively. This assignment predicts an intense ν_0 transition at 0.5 MHz. It can be seen from figure 2(b) that such a transition was indeed observed. The quadrupole coupling constant e^2qQ/h and the asymmetry parameter η are estimated to be around 2.0 MHz and 0.5, respectively. The assignments made, however, are not unambiguous as there are a number of lines unaccounted for, and also it is known that a line at low frequency (0.5 MHz) can sometimes appear due to instrumental artefacts in three-pulse experiments. This aspect can possibly be clarified from hyperfine sublevel correlation (HYSCORE) spectra [32–35] by conducting 2D four-pulse experiments. These aspects are discussed in section 3.3.

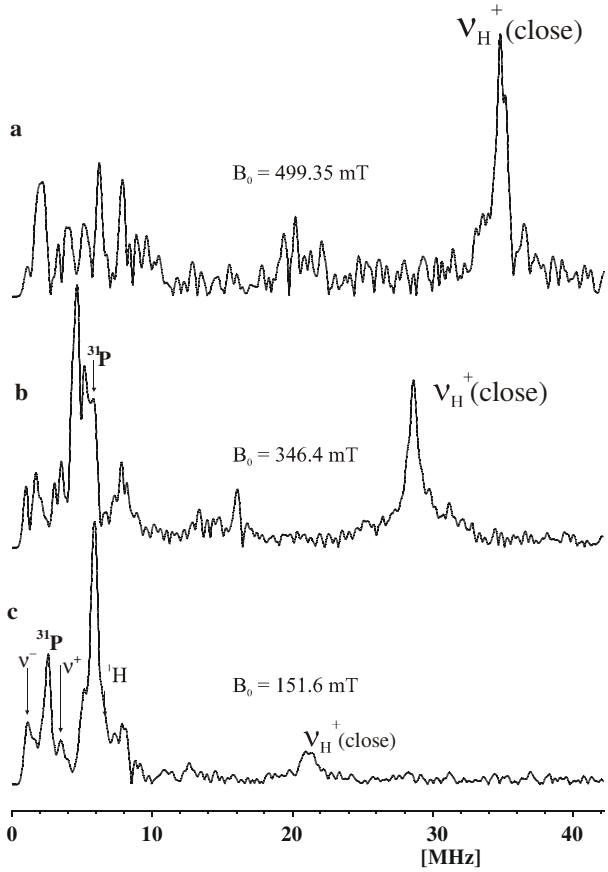

Figure 3. The FT of three-pulse ESEEM of AsO_4^{4-} in RDP for three different hyperfine components at fields shown in the figure. The ν^+ component of close ^{1}H coupling is shown. The lines at low frequency in (a) are due to interaction with ^{85}Rb and ^{87}Rb.

3.2.2. Rubidium dihydrogen phosphate (RDP) single crystal. The FT spectra of three-pulse ESEEM for AsO_4^{4-} in RDP using echoes of three different hyperfine transitions are shown in figures 3(a)–(c). The most prominent feature of these spectra is the coupling with hydrogen in O–H$\cdots$O networks with ν_H^+ at 35 MHz for a static field of 499.3 mT. The proton lines shifted to different frequencies as expected at different field strengths. The coupling constant of this interaction is estimated to be 27 MHz, from this ENDOR-like spectrum (this is in agreement with the values reported for hyperfine interaction with protons along the *c*-axis) [18]. The interaction with ^{31}P was clearer at low field (151.6 mT) and intermediate field (346.4 mT). The lines marked $\nu^\pm$ in figure 3(c) around the ^{31}P line are tentatively assigned to ^{31}P interaction. There are a number of lines in the low frequency range, most probably due to interaction with ^{85,87}Rb. The assignments of hyperfine lines to quadrupolar nuclei are not straightforward. These aspects are discussed in section 3.2.4 while presenting the ESEEM of powder RDP samples.

3.2.3. RADP single crystal and comparison with RDP and ADP. The ESEEM spectra obtained in RADP ($x = 0.5$) gain greater significance on comparing with the spectra obtained

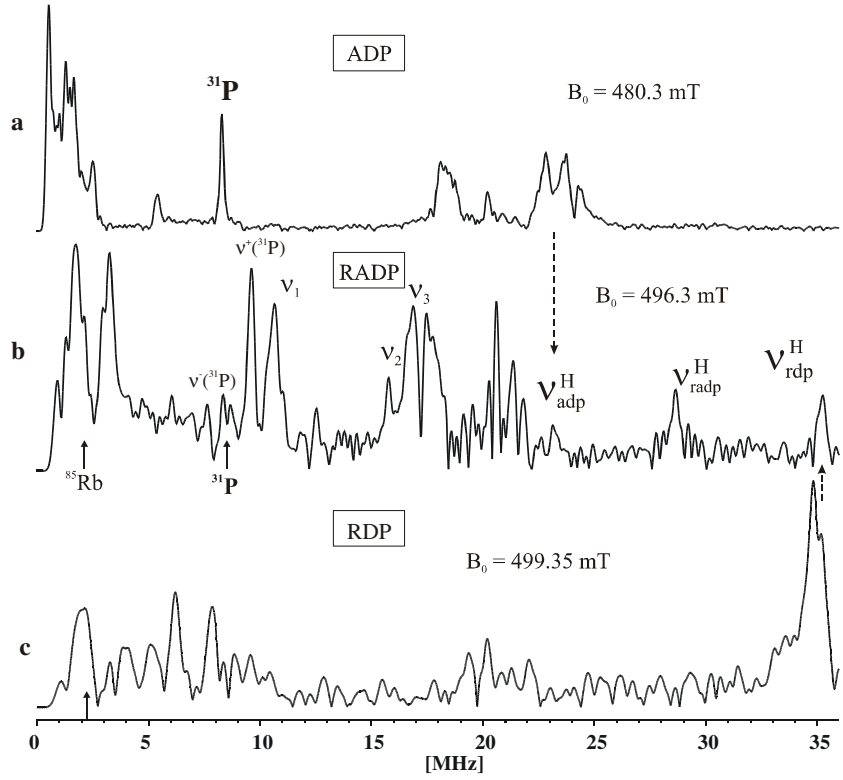

Figure 4. The FT of three-pulse ESEEM of the highest field line of the AsO_4^{4-} radical in (a) ADP, (b) RADP and (c) RDP. In (b) it can be seen that ν^H_{adp} and ν^H_{rdp} are observed along with ν^H_{radp}. The lines marked ν_1, ν_2 and ν_3 are the combination lines. $\nu_1 = \nu(^{31}P) + \nu(^{85}Rb)$; $\nu_2 = \nu(^{31}P) + \nu(^{87}Rb)$; $\nu_3 = 2\nu(^{31}P)$. $\nu^-(^{31}P)$ agree with ENDOR assignments in KDP [18]. The signal at 12.5 MHz, observed only in RADP, is close to the expected low frequency component, ν^{H-}_{radp}, at 13.7 MHz (see the text).

in pure ADP and RDP, as this might lead to an understanding of the mechanism of glass formation. Figure 4(b) shows the FFT of three-pulse ESEEM obtained with the high field line of AsO_4^{4-} in RADP and the corresponding spectra obtained in RDP and ADP are also included (figures 4(a) and (c) respectively) to enable easy comparison of the features. It may be noted that the ESEEM spectrum of RADP consisted of signals due to interaction with proton observed in RDP around 34.5 MHz and in ADP at 23 MHz (marked as ν^H_{rdp} and ν^H_{adp} respectively) along with a new signal, marked ν^H_{radp} at 28.5 MHz. This appeared close to the centre of the corresponding lines for RDP and ADP. The Larmor frequency of a proton at 496.3 mT would be 21.13 MHz. The low frequency signal corresponding to ν^{H+}_{radp} is expected around 13.76 MHz. The signal that came closest to this frequency in RADP is at 12.5 MHz. Its absence in ADP and RDP (figures 4(a) and (c)) suggests that it can possibly be due to ν^{H-}_{radp}. However, in 1D ESEEM of powder RDP, a signal was observed around 12 MHz (see figure 5). In view of this it is difficult to firmly identify this signal. It may be important to remark here that suppression effects in ESEEM and HYSCORE spectra are not uncommon in multinuclear spin systems, particularly of ^{1}H peaks in the presence of strong ^{14}N peaks, as shown by Stoll *et al* [36]. These authors have shown that in multinuclear systems there

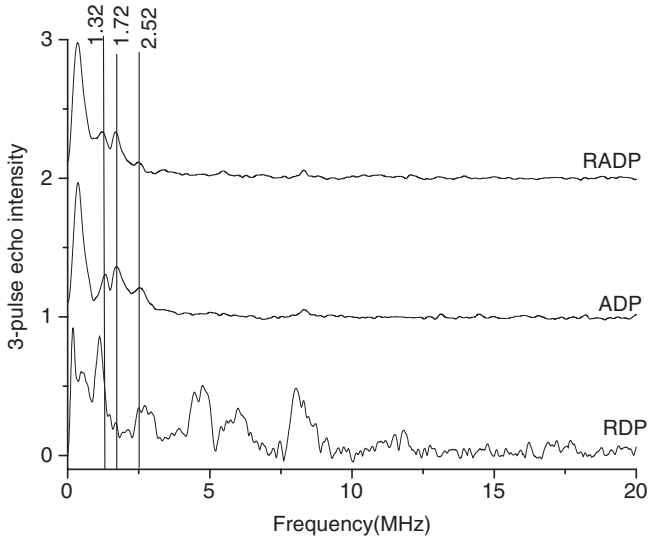

Figure 5. Three-pulse ESEEM spectra of ADP, RADP and RDP powder samples with the magnetic field locked on to the highest field ^{75}As hyperfine line of AsO_4^{4-}. The spectrum obtained at 40 K was obtained by adding measurements with $\tau = 200$, 248 and 300 ns to avoid blind spots.

is a significant interplay between the modulation depth and the blind-spot term of one group of nuclei on the other group, resulting in strong suppression of peaks of nuclei with shallow modulation by those with deep modulations. It may be seen from figure 4(b) that there are many intense lines in the 10–20 MHz range, close to 13 MHz where $\nu_{\mathrm{radp}}^{\mathrm{H}-}$ is expected. This was probably responsible for the suppression of the ^{1}H line in this range. The absence of intense lines from other nuclei beyond 20 MHz facilitated the observation of $\nu^{\mathrm{H}+}$ lines in all three matrices. Additional features, assigned to some combination lines, are marked in figure 4(b).

3.2.4. Three-pulse ESEEM on powdered samples. Spectra of ADP, RDP and RADP obtained with different $T = 200$, 248 and 300 ns in the pulse sequence $\pi/2$–T–$\pi/2$–τ–$\pi/2$ were added together to eliminate the possibility of blind spots. The three-pulse ESEEM powder spectra conducted on the highest field line of AsO_4^{4-} in ADP, RDP and RADP are shown in figure 5. The FT of ESEEM obtained in ADP revealed an intense line at 0.35 MHz and three prominent lines with maxima at 1.32, 1.72 and 2.52 MHz. The appearance of this powder spectrum, nearly as well resolved as that from the single crystal, supports the conclusion that these lines in the low frequency range are obtained from the interaction with the ^{14}N nuclear quadrupole under the cancellation condition $A_{\mathrm{iso}} \approx 2\nu_N$. It is interesting to note that the coupling constants obtained for ^{14}N are typically like those obtained in irradiated nitrates and amine groups of amino acids [29–31]. In ADP and RADP, a weak line was observed around 8.0–8.5 MHz. It is most likely due to ^{31}P. It is rather intriguing why the ^{31}P line could be seen in RADP powder, when it was absent in single crystals. One distinct possibility could be the partial loss of ammonium during sample grinding, making the sample slightly Rb-rich.

In the case of RDP a number of broad lines appeared in the 0.5–8 MHz range, both for single-crystal and powder samples, most likely due to interaction with 72% abundant ^{85}Rb ($I = 5/2$, quadrupole moment $Q = 0.273|e| \times 10^{-24}$ cm^2, nuclear Larmor frequency of 1.980 MHz at 480 mT) and 22% abundant ^{87}Rb ($I = 3/2$, quadrupole moment $Q = 0.130|e| \times 10^{-24}$ cm^2, nuclear Larmor frequency of 7 MHz at 480 mT). Whereas the ESEEM spectra in general are

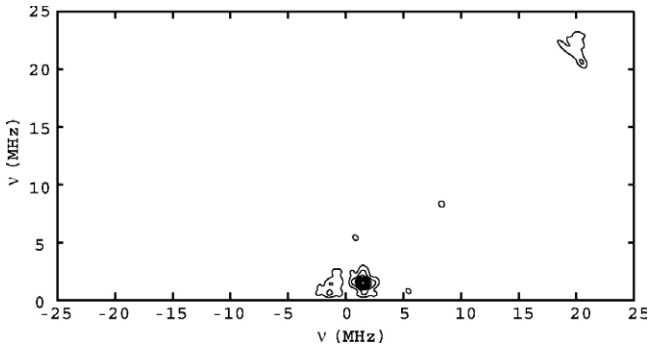

Figure 6. HYSCORE powder spectrum of RADP with the magnetic field locked on to the highest field ^{75}As hyperfine line of AsO_4^{4-}. The spectrum obtained at 20 K was obtained by adding measurements with $\tau = 200$, 248 and 300 ns to avoid blind spots.

well resolved for $I = 1/2$ and 1 nuclei (under the cancellation condition), the ESEEM spectra get quite complicated for nuclei of spin $I \geqslant 3/2$ [37, 38]. Ponti [39] has examined this aspect in great detail for an arbitrary spin. He has shown that the spin echo modulation amplitudes are polynomials of degree $2I$, in the modulation depth parameter k. This results in the appearance of harmonics of the fundamental modulation up to the $2I$th in the ESEEM with amplitudes comparable to the fundamental. The presence of strong quadrupole interaction would further complicate the spectra. It is quite possible that many lines in the low frequency range in RDP arose due to some of these factors, with both isotopes of Rb having large nuclear spin and quadrupole moments. In view of this, no attempt is made to assign the low frequency lines in RDP, both for powder and single-crystal samples.

3.3. HYSCORE spectra of ADP, RDP and RADP

The HYSCORE data were obtained to get unambiguous information on interactions in the low frequency range [32–35] compared to three-pulse ESEEM. Hyperfine interaction due to ^{14}N, ^{31}P, ^{85,87}Rb and distant ^{75}As are covered in this range, the most important of them being ^{14}N. As mentioned earlier, when the hyperfine coupling constant is about twice the nuclear Larmor frequency, a zero effective field is experienced by the nucleus in one of the electron spin manifolds (cancellation condition) with ESEEM frequencies corresponding to pure NQR frequencies. This electron spin manifold is referred to as a low effective field manifold (LEF) and the other as the high effective manifold (HEF) [35]. If indeed the cancellation condition is satisfied, the ESEEM frequencies in the LEF would appear as spots on the diagonal in one or both of $(+,+)$ and $(-,+)$ quadrants in the HYSCORE spectra. The hyperfine structure from the HEF would appear as cross-peaks correlated to these NQR-like peaks on the diagonal. The cross-peak intensity may be distributed between the two $(+,+)$ and $(-,+)$ quadrants of the HYSCORE spectrum [34, 35]. Spectra of RADP powder obtained with $\tau = 200$, 248 and 300 ns for the HYSCORE pulse sequence $\pi/2$–τ–$\pi/2$–t_1–π–t_2–$\pi/2$–τ-echo were added together to eliminate the possibility of blind spots. The spectrum shown in figure 6, with the magnetic field locked on to the highest field ^{75}As hyperfine line of AsO_4^{4-}, contains pronounced features assigned to ^{14}N LEF in the $(+,+)$ and $(-,+)$ quadrants. Weak spots attributed to ^{14}N HEF appeared symmetrically about the diagonal in the $(+,+)$ quadrant, while the features on or near the diagonal at about 8 and 21 MHz are those expected for weakly coupled ^{31}P and ^{1}H nuclei. The features are relatively poorly resolved, however, particularly in the low frequency

region. The contours overlapping with a spot centred around 2 MHz (^{14}N) are extended parallel to the diagonal in the (+, +) quadrant up to 3–3.5 MHz. The HYSCORE spectra obtained for single crystals of RDP, ADP and RADP with magnetic field parallel to the *c*-axis and locked on to the highest field ^{75}As hyperfine line of AsO_4^{4-} were therefore examined in the low frequency region to obtain clearer information. The HYSCORE spectra of RDP, ADP and RADP single crystals, obtained at 40 K, are shown in figures 7(a)–(c) respectively. The data obtained for ADP and RADP in the low frequency range, 0–4 MHz, contained interesting and significant information about ^{14}N interaction. The HYSORE data on RDP contained peaks on the diagonal, corresponding to weakly interacting nuclei.

In the case of ADP, intense peaks around 0.5 MHz with contours spreading from 0.25 to 0.7 MHz were observed on the diagonals of both the quadrants. In addition to this, on the diagonal of the (+, +) quadrant three closely spaced spots with contours spreading in the direction perpendicular to the diagonal were observed at 1.5, 1.75 and 2.0–2.2 MHz, the most intense among them being the one at 1.5 MHz. The harmonics of 1.75 and 2.0 MHz peaks were observed at 3.5 and 4.0 MHz respectively on the same diagonal. The fundamental peaks on the diagonal are due to NQR-like transitions arising from the LEF manifold under the cancellation condition. These are consistent with the three-pulse ESEEM spectra discussed earlier; slight frequency differences might be due to crystal orientation differences. A striking observation is the appearance of intense cross peaks correlated to the 0.5 MHz peak of the LEF manifold, at two close-by frequencies (0.5, 3.0) and (0.5–0.7, 3.2) in both quadrants. Further, less intense cross peaks were observed at (0.5, 6.2) and (0.7, 6.0) in the (+, +) quadrant. One set of lines disappeared on the formation of RADP, in which the HYSCORE spectral features are much simpler (see figure 7(c)). These observations clearly show that the ammonium ion exists in two different forms of distortion and gets reduced to only one form on the formation of the mixed compound RADP. The NQR-like frequencies in the LEF manifold for the two sites are as follows. For site I: $\nu_0 = 0.2$–0.5, $\nu_- = 1.5$ and $\nu_+ = 1.75$–1.8 MHz; for site II: $\nu_0 = 0.5$–0.6, $\nu_- = 1.5$ and $\nu_+ = 2.0$–2.1 MHz. This yields values of $e^2qQ/h = 2.2$ MHz and $\eta \sim 0.27$ for site I and 2.33 MHz and 0.42 respectively for site II. The A_{iso} values were estimated to be around 2.7–2.8 MHz, taking the intense cross peak in the 3.0–3.25 MHz range as the lower single quantum transition in the HEF. These values (for both sites I and II) appear to be quite reasonable as they are in the range satisfying the cancellation condition. The peak at 6.5 MHz on both diagonals is most likely due to combinations of frequencies in the HEF manifold, due to the presence of two inequivalent nitrogens in ADP, which disappear on the formation of RADP. The diagonal peaks around 8 MHz in both quadrants are due to ^{31}P. The intense peaks observed around 10–12 MHz were assigned to combination lines. In the case of RDP, in addition to a sharp peak around 8 MHz corresponding to a nuclear Larmor frequency of ^{31}P, intense peaks with broad and extended contours between 2.75 and 4.2 MHz were observed which are most likely due to 72% abundant ^{85}Rb ($I = 5/2$) with large quadrupole interaction. Table 1 gives the frequencies of peaks obtained on the diagonals that include the pure NQR frequencies and also those due to weakly coupled distant nuclei. It may also be mentioned that some of the peaks on the diagonal could also be due to an incomplete excitation of the recovery pulse in the experiment. Table 2 gives the frequencies of cross-peaks, symmetrically located with respect to the diagonal. As no cross-peaks were observed in RDP, it is not included in table 2.

3.4. Phase memory time, T_M, measurements

We have obtained data on T_M for the paramagnetic AsO_4^{4-} centre in RDP, ADP and more extensively in RADP using two-pulse experiments. The phase memory time T_M data were obtained by exponential fitting of two-pulse ESE decays, in the temperature range 20–200 K.

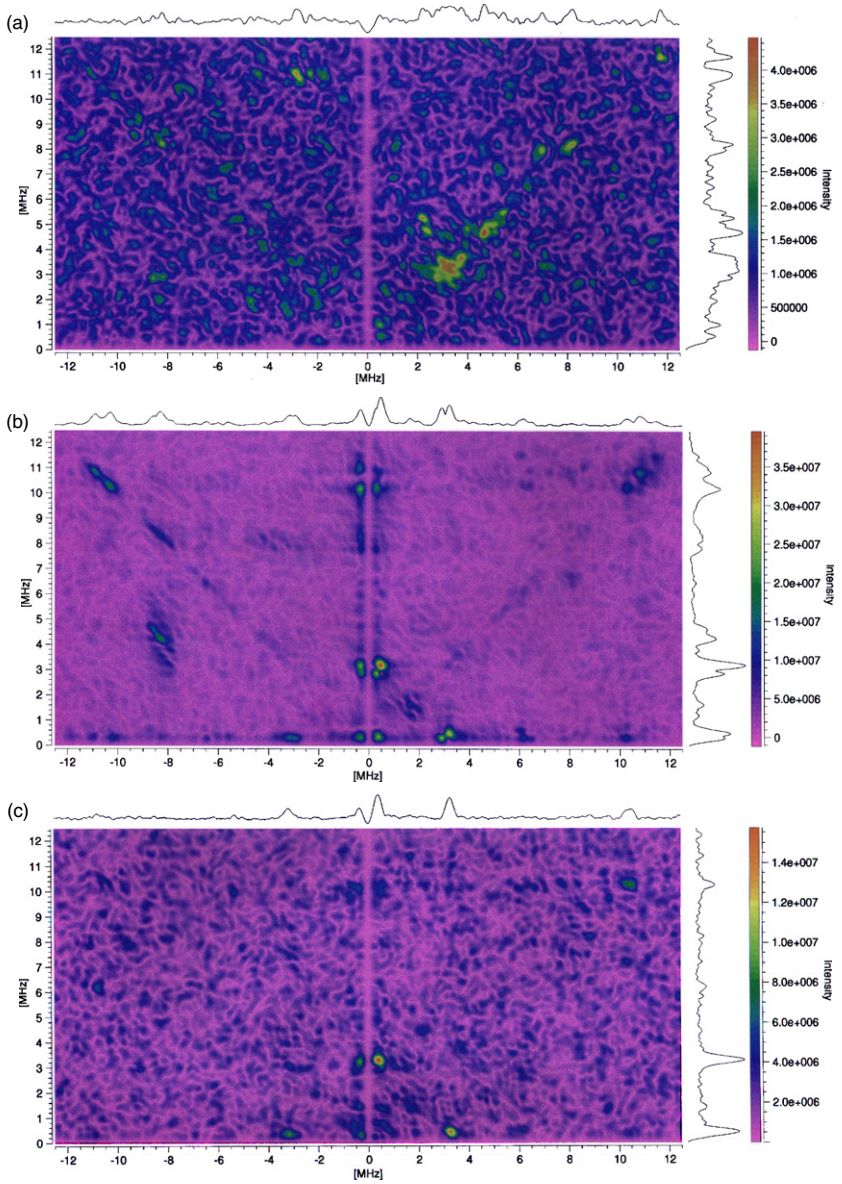

Figure 7. (a) HYSCORE spectrum at 40 K of the low frequency range for a single crystal of RDP, with the magnetic field locked on to the highest field ^{75}As hyperfine line. The magnetic field is slightly off the *c*-axis (about 5°). Most of the signals (spots) are on the diagonal in the (+, +) quadrant, indicating weak interaction. The assignments are listed in table 1. (b) HYSCORE spectrum of ADP single crystals at 40 K. The other conditions are identical to that given in (a). The observation of two spots correlated to the ^{14}N frequency suggests the existence of two inequivalent nitrogens. The assignments are given in tables 1 and 2. (c) HYSCORE spectrum of an RADP single crystal at 40 K, under the same conditions as in (a) and (b). The disappearance of one set of spots assigned to ^{14}N, on the formation of dipolar glass RADP, may be clearly noted (compare with (b)). The assignments made are given in tables 1 and 2.

The data obtained for different hyperfine components of AsO_4^{4-} in RADP are shown in figure 8. The phase memory time was found to depend upon the nuclear spin quantum number of ^{75}As,

Table 1. The HYSCORE spectral line positions, in units of MHz, on the diagonals of both quadrants for RDP, ADP and RADP. These spectral features reveal interaction with weakly coupled nuclei and pure quadrupole interaction for ^{14}N in the LEM under cancellation condition. (s—strong, vs—very strong, w—weak, s&b—strong and broad.)

RDP (+, +)	RDP (−, +)	ADP (+, +)	ADP (−, +)	RADP (+, +)	RADP (−, +)	Assignment
—	—	0.25–0.6 (s)	0.25–0.6 (s)	0.25–0.7 (w)	0.25	^{14}N (ν_0)
—	—	1.5 (s)	—	—	—	^{14}N (ν^-)
—	—	1.75 (vs), 2.0	—	2.0	2.0	^{14}N (ν^+)
—	—	3.5–4.0	3.75–4.25	3.75	3.0–3.5	^{14}N (double quantum)
2.7–4.0 (wide contours)	—	—	—	—	—	^{85}Rb with quadrupole interaction
5–6 (s&b)						(^{31}P–^{85}Rb) diff. freq.
—	—	6–6.5	6.5	—	—	(^{31}P–^{14}N) diff. freq.
8–8.5 (vs)	8.25 (s)	8.3 (w)	7.5–8.5 (s)		—	^{31}P
—	—	10.25 (vs)	10.0	10.5 (s)	10.25 (w)	(^{31}P + ^{14}N) sum freq.
—	—	11.5 (s)	11.0	—	—	(^{31}P + 2^{14}N)?
11.5	—	—	—	—	—	(^{31}P + ^{85}Rb) sum freq.

Table 2. Cross-peaks observed in ADP and RADP in respective quadrants. As the cross-peaks are symmetric about the diagonal, only one of the pairs is listed. The coordinates are in MHz (Sq = single quantum, Dq = double quantum).

ADP (+, +)	ADP (−, +)	RADP (+, +)	RADP (−, +)	Assignments
(2.8, 0.4)	(−0.5, 2.8)	—	—	^{14}N (site I). Sq transition in HEF
(3.2, 0.6)	(−0.6, 3.2)	(3.2, 0.4)	(−0.4, 3.2)	^{14}N (site II)
		(0.5, 6.0)		Double quantum transition in HEF manifold
—	(−4, 8)	—	—	(^{31}P + Dq of ^{14}N)?

and it showed an interesting temperature dependence with a prominent anomaly around 90 K. These interesting findings will be discussed in section 4.2. The temperature dependences of T_M of the high field components of the AsO_4^{4-} radical in ADP and RDP are shown in figure 9. In the case of RDP a large spread in T_M was observed, presumably due to its polar ordering and thereby higher sensitivity to temperature fluctuations. Whereas the T_M value in RDP is relatively larger and monotonically increased with lowering of temperature, the T_M in the ADP matrix exhibited a sharp anomaly at the AFE-phase transition at 145 K, and also a striking anomaly around 60 K. The temperature dependence of T_M for the high field component in RADP is also included in figure 9, for comparison.

4. Discussion

The new experimental findings may be classified under two categories: (i) structural information relating to the ammonium ion, obtained through hyperfine interaction with ^{14}N, and (ii) information about the nature of dipolar glass formation in the mixed compound of RDP and ADP, namely RADP, as derived from the temperature dependence of the phase memory time T_M, and proton hyperfine structure in 1D three-pulse ESEEM measurements.

4.1. Hyperfine interaction with ^{14}N and structure of the ammonium ion in ADP and RADP

The hyperfine interaction of the unpaired electron in the AsO_4^{4-} radical with ^{14}N in ADP is observed in the present three-pulse ESEEM study, both in single-crystal and powder forms,

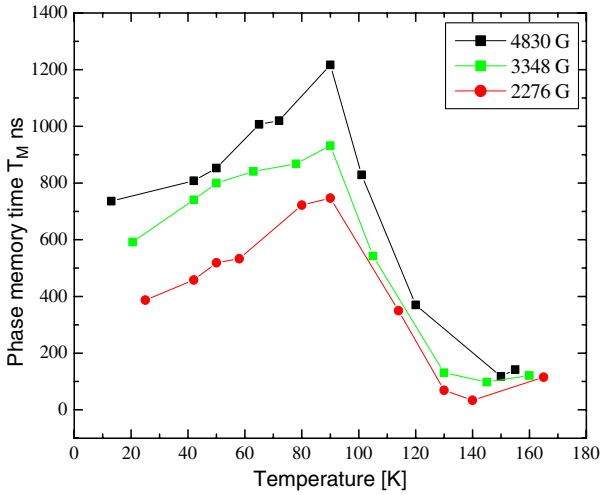

Figure 8. The temperature dependence of phase memory time T_M of the AsO_4^{4-} radical in an RADP single crystal with magnetic field 5° off the *c*-axis. Measurements were done using two-pulse ESE decay for different hyperfine components (resonance fields are marked). A clear anomaly at 90 K can be seen.

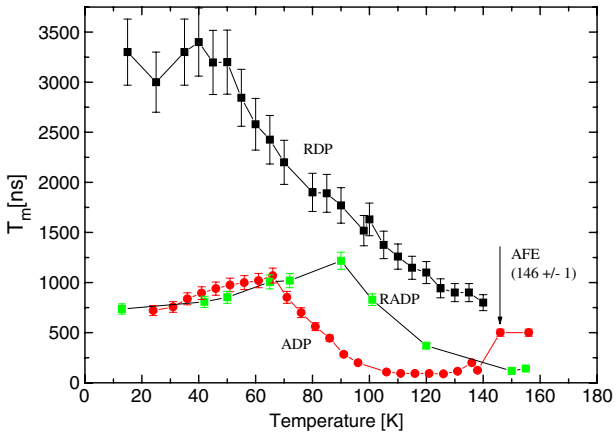

Figure 9. The temperature dependence of phase memory time T_M of the AsO_4^{4-} radical in RDP and ADP, for the high field line with magnetic field 5° off the *c*-axis; the corresponding data for RADP are also included for ready comparison.

and is clearly confirmed by four-pulse HYSCORE spectral investigation. This information was missed in earlier ENDOR studies, most likely due to the low frequencies where the interaction is observable. The cancellation condition attained at 480.3 mT created a favourable situation for the observation of pure NQR-like lines in the LEF, and the magnetic hyperfine interaction in the HEF. Powder ESEEM results and more strikingly HYSCORE spectra have shown that the ammonium ion exists in two distorted forms in ADP, out of which only one was found to survive on the formation of RADP.

4.2. The temperature dependence of phase memory time

The two-pulse ESE decay is characterized by T_M, with its FT defining the homogeneous line shape of an individual spin packet with a half-width at half-intensity corresponding to the reciprocal of the phase memory time T_M. Since this homogeneous spin packet width can be several orders of magnitude smaller than the width of the inhomogeneously broadened EPR line, it is more sensitive to time-dependent local fields. There can be various contributions to the phase memory time T_M, which include the spin–lattice relaxation time T_1, spin–spin relaxation time T_2 and nuclear spin–spin relaxation causing nuclear spin flips. All these arise due to local field fluctuations and their relative contributions depend upon a given physical situation [27]. The significance of phase memory time, and its temperature dependence, were discussed extensively by Brown [27], Schwartz *et al* [40] and Hoffmann *et al* [41]. As the local field fluctuations arise due to dynamic processes, the temperature dependence of T_M can be used to monitor the molecular dynamics of the probe ion and/or that of matrix molecular units. At low radical concentrations, the values of T_M are independent of radical concentrations and usually depend on the matrix [27]. Schwartz *et al* [40] simulated the ESE decays using the time-dependent stochastic Liouville equation and provided a method for studying very slow molecular motions. This work had shown that $T_M(T)$ goes through a minimum as one goes through a fast to slow motion regime. The results obtained in the present investigation (figures 8 and 9) are in contrast with those reported by Schwartz *et al* [40] for slow molecular motion in solutions. Hoffmann *et al* [41] have extensively discussed the possible manifestations of various physical phenomena causing phase memory relaxation in the mathematical form of ESE decay, and also the nature of the temperature dependence of T_M and applied it to the Jahn–Teller Cu^{2+} complex in Tutton salt single crystals. They have shown that the dominant $\exp(-b\tau)$-type decay reflected the role of fast spectral diffusion under dynamical line narrowing conditions and/or the exchange-type process between two frequencies, and $\exp(-m\tau^2)$-type decay suggested the role of nuclear spin diffusion through a flip-flop process. All the ESE decays in the present study gave a satisfactory fit with a single exponential with a linear term suggesting the possible existence of dynamical line narrowing conditions and their role in phase memory relaxation. Among the three lattices investigated the phase memory time for the arsenate radical is the longest in RDP, and it monotonically increased with lowering of temperature, i.e. the dephasing rate decreased with lowering of temperature, having a value of $\sim 3 \times 10^5\ s^{-1}$ at 30 K. The results for ADP are somewhat similar to those of $T_{1\rho}$ (spin–lattice relaxation in the rotating frame), reported for pulsed proton NMR in ADP [42]. The values of $T_{1\rho}$ are expected to be sensitive to very slow fluctuations and the NMR results gave evidence for slowing down of two-fold hindered rotation of the ammonium group, and associated distortion.

The temperature dependence of T_M in RADP is expected to reflect the dynamical processes that become manifest due to competing interaction in an FE–AFE mixed system. In the case of RADP, T_M progressively increased with decreasing temperature below 145 K, the temperature at which RDP and ADP undergo FE and AFE phase transitions respectively, peaking at 90 K, coinciding with the temperature of onset of freezing [6]. Hoffmann *et al* [41] have shown that when spin dephasing is dominated by a T_1 process, the dephasing rate $1/T_M$ decreases with lowering of temperature i.e. T_M increases with lowering of the temperature, and a reverse trend was predicted if spin dephasing was controlled by the motion of molecules, containing magnetic nuclei, in the lattice (see figure 8 in [41]). The motions (jumps, rotations and librations) of paramagnetic molecular ions having g and A anisotropy were identified as a dominant contributor to the T_1 process and thereby to slower spin dephasing with lowering of the temperature. The AsO_4^{4-} molecular ions in RDP (FE) and ADP (AFE) have different hyperfine coupling constants, the differences being of the order of 30–50 MHz [21]. A fluctuation

between FE and AFE configurations close to AsO_4^{4-} molecular ions would be equivalent to a jump of the probe ion between FE and AFE configurations in RADP. The increase of $T_M(T)$ below 145 K, the FE transition temperature, down to 90 K, the glass freezing temperature, strongly suggests that the T_1-process arising due to FE $\leftrightarrow$ AFE fluctuations predominantly contributes to spin dephasing in this temperature range when the constituents of RADP entered a regime of mutually competing order. Therefore, the temperature dependence of T_M shown in figures 8 and 9 clearly reflects the onset of new dynamics as RADP enters the glassy phase and it progressively slows down below 90 K. Around this temperature the FE $\leftrightarrow$ AFE fluctuation rate gets slower than the inverse of $(A_{adp} - A_{rdp})$ in frequency units ($\sim 0.2 \times 10^{-7}$ s), and the T_1 process ceases to be the most dominant spin dephasing process below this temperature, being overtaken by lattice molecular motion with correlation time $\tau_c > 0.2 \times 10^{-7}$ s. The slow fluctuations in the proton ordering between FE and AFE configurations could be the only source of lattice molecular motion that could contribute to spin dephasing. If this fluctuation were not present T_M would have been temperature independent below 90 K.

4.3. Dipolar glass formation

It is well established that RDP transforms into the ferroelectric phase around 145 K, and ADP into the antiferroelectric phase at around the same temperature; and in view of the equal sizes of rubidium and ammonium ions they form a solid solution over a wide concentration range, and the mixed salt exhibits the formation of a dipolar glass. What sets dipolar glasses (or spin glasses) apart from conventional broken symmetry systems is broken ergodicity, expected to be caused by frustration combined with intrinsic disorder in the system [1]. The problem addressed is whether the glass formation is associated with random static distributions of local ferroelectric and antiferroelectric phases or if there are dynamical features associated with competing interactions which get slowed down leading to a completely static situation at much lower temperatures. The former case can possibly be categorized under a non-ergodic system wherein each individual site need not describe the bulk property, whereas the dynamic model represents an ergodic state of the system.

The experimental findings of relevance to understand the possible mechanism of dipolar glass formation are: (i) the appearance of proton hyperfine interaction in RADP midway between those of ADP and RDP, along with those features observed in pure RDP and ADP; (ii) interesting temperature dependence of T_M in the case of RADP, exhibiting m_I dependence and anomalous behaviour at 90 K coinciding with the temperature of onset of freezing in RADP given by Courtens [6], and (iii) the temperature dependence of T_M in ADP exhibiting marked features, presumably reflecting the changes in the molecular dynamics of the ammonium group as there are some similarities with the temperature dependence of a proton $T_{1\rho}$ in ADP [41].

The appearance of a proton hyperfine line in RADP at the average value of the constituents is a clear pointer to the existence of dynamic fluctuation. The concomitant presence of separate RDP and ADP features (with regard to the ^{1}H hyperfine structure) in RADP could have led to the conclusion that RADP does contain local RDP- and ADP-rich regions. However, from the absence of intense lines due to ^{31}P and ^{85}Rb in RADP (in contrast to ADP and/or RDP) and also ^{14}N lines from site I, both in ESEEM and HYSCORE, it can be concluded that RADP does not have regions of static inhomogeneities with ammonium/rubidium-rich regions. From these features it may be possible to estimate the spread in correlation time of FE–AFE fluctuations. The difference in the positions of υ^{H+} lines in ADP and RDP is around 12 MHz. If there are fluctuations with correlation time shorter than the inverse of this frequency, namely 0.8×10^{-7} s, the condition for exchange narrowing would be satisfied, resulting in the presence of an averaged spectrum in RADP. If there is a spread in the correlation times, covering time

scales longer than 0.8×10^{-7} s, separate ADP and RDP features can be seen in the proton structure along with RADP features. The absence of a ^{31}P signal in ESEEM and HYSCORE of RADP which is prominent in ADP, however, suggests that dynamic fluctuations with a frequency around 8.5 MHz could be present, broadening the ^{31}P line beyond recognition. This implies the presence of a fluctuation with a correlation time equal to or shorter than 1.2×10^{-7} s. This is slightly larger than the value 0.8×10^{-7} s obtained above as a limiting time scale for fluctuation satisfying the averaging criterion. This is consistent with the appearance of $\nu^{\mathrm{H}}_{\mathrm{adp}}$ and $\nu^{\mathrm{H}}_{\mathrm{rdp}}$ along with $\nu^{\mathrm{H}}_{\mathrm{radp}}$ in RADP. Even under the condition that these features in figure 4(b) reflected static inhomogeneities or impurity phases (the word 'impurity' is used to mean those regions where a homogeneous solid solution of the basic constituents may not have formed in RADP), $\nu^{\mathrm{H}}_{\mathrm{radp}}$ is a characteristic fingerprint of RADP which is distinctly different from those of pure end members in the phase diagram, namely RDP and ADP, and is a signature of dynamic averaging of FE and AFE phases.

4.4. Is it a case of broken ergodicity?

As mentioned earlier, there are formal similarities between spin glasses and dipolar glasses, and ergodicity (or broken ergodicity) defines the state of the system. Venkataraman *et al* [43] and Fischer and Hertz [44] have discussed some important aspects of broken ergodicity in these materials. If τ_0, the time scale of observation, is adequate to give the same averages as would be obtained for much longer times of observation, the system can be considered to be ergodic even though the observations are made on a finite time scale τ_0. One would enter the regime of broken ergodicity if there exist dynamic processes with time scales much longer than τ_0, conventionally of the order of years, i.e., in situations of practically frozen fluctuations. In a spin glass or dipolar glass, in the framework of the Ising model and fluctuating ferro- and antiferromagnetic/electric interactions, the Hamiltonian can be represented in the form [43]

$$H = J \sum_{ij} \sigma_i A_{ij} \sigma_j \tag{2}$$

($A_{ij} = \pm 1$ is a random variable which includes the random fluctuations of exchange integral between $\pm J$). The A_{ij}s are bond parameters at the corresponding sites and do not undergo thermal fluctuations, in the time scale of observation, in contrast to the spin variables σ_{ij}. The glassy states are those situations in which A_{ij}s are frozen or quenched random variables, and every frozen configuration 'A' breaks the ergodicity [43]. In the context of RADP, the dipolar interactions have to be considered in a highly polarizable medium, which can induce a glass-like relaxor state, and the A_{ij} represent the random variations in the surroundings of dipoles, which mediated ferro- and antiferroelectric interactions. The ESEEM results presented above, with regard to the hyperfine interactions with the proton in the O–H$\cdots$O bond, show that the observable, namely the strength of hyperfine coupling, is indeed the average over the possible distributions in A_{ij}, and it remains so down to 20 K. In the case of static distribution of different configurations a well-defined line marked $\nu^{\mathrm{H}}_{\mathrm{radp}}$, would not have been detectable. This observation and the earlier experimental findings of Babu *et al* [21, 23] that the hyperfine constant of the AsO_4^{4-} radical in RADP was the weighted average of the respective RDP and ADP phases, are in agreement with ergodic R-state of the system, as proposed by Samara [1, 9] from dielectric measurements, in the temperature and frequency range used.

5. Conclusions

ESEEM, HYSCORE and phase-memory time, T_{M}, measurements on the paramagnetic AsO_4^{4-} radical in RDP, ADP and the dipolar glass RADP ($x = 0.5$), gave clear evidence for the

following: (i) the ammonium ion exists in two distorted forms in antiferroelectric ADP, whereas it takes a unique position on the formation of RADP, and (ii) FE–AFE fluctuations exist below 150 K, in the glassy phase, going through a maximum at 90 K. These fluctuations have correlation times in the 0.2×10^{-7}–1.2×10^{-7} s range. The RADP system therefore appears to be in an ergodic R-state above 20 K.

Acknowledgment

MDS wishes to acknowledge the financial support received from the Wenner-Gren foundation in the form of a visiting professorship.

References

[1] Samara G 2001 Ferroelectricity revisited—advances in materials and physics *Solid State Physics—Advances in Research and Applications* vol 56, ed H Ehrenreich and F Spaepen (New York: Academic) p 239
[2] Binder K and Young A P 1986 *Rev. Mod. Phys.* **58** 8011
[3] Höchli U T, Knorr K and Loidl A 1990 *Adv. Phys.* **39** 405
[4] Courtens E 1982 *J. Phys. Lett.* **43** L199
[5] Courtens E 1983 *Helv. Phys. Acta* **56** 705
[6] Courtens E 1987 *Ferroelectrics* **72** 229
[7] Slak J, Kind R, Blinc R, Courtens E and Zumer S 1984 *Phys. Rev.* B **30** 85
[8] Moussa F and Courtens E 1991 *Ferroelectrics* **17** 347
[9] Samara G A 1991 *Ferroelectrics* **117** 347
[10] Hampton M A, Herring F G, Lin W C and McDowell C A 1966 *Mol. Phys.* **10** 565
[11] Dalal N S, Dickinson J R and McDowell C A 1972 *J. Chem. Phys.* **57** 4254
[12] Dalal N S, McDowell C A and Srinivasan R 1972 *Mol. Phys.* **24** 417
[13] Gaillard J, Constantinescu O and Lamotte B 1972 *J. Chem. Phys.* **55** 5447
[14] Dalal N S 1982 *Adv. Magn. Reson.* **10** 119
[15] Sampaio J F, Ribeiro G M, Chaves A S and Gazzinelli R 1986 *J. Phys. C: Solid State Phys.* **19** 7269
[16] Muller K A 1987 *Ferroelectrics* **72** 273
[17] Kahol P K and Dalal N S 1988 *Solid State Commun.* **65** 823
[18] Dalal N S and Kahol P K 1989 *Solid State Commun.* **70** 623
[19] Kahol P K, Lao X, Williams M E and Dalal N S 1994 *Phys. Rev.* B **49** 9176
[20] Rakvin B and Merunka D 1997 *J. Magn. Reson.* **126** 87
[21] Babu Y, Sastry M D and Dasannacharya B A 1992 *J. Phys.: Condens. Matter* **4** 1819
[22] Kahol P K, Lao X, Costello M B and Dalal N S 1994 *J. Phys.: Condens. Matter* **6** 2971
[23] Babu Y, Sastry M D and Dasannacharya B A 1994 *J. Phys.: Condens. Matter* **6** 2975
[24] Xu R, Kahol P K and Dalal N S 1994 *Ferroelectrics* **156** 377
[25] Klymachyov A N, Xu R, Wandelt A, Kahol P K and Dalal N S 1996 *Phys. Rev.* B **53** 6123
[26] Barkhuijsen H, de Beer R, Deutz A F, van Ormondt D and Völkel G 1984 *Solid State Commun.* **49** 679
[27] Brown I M 1979 *Time Domain Electron Spin Resonance* ed L Kevan and R N Schwartz (New York: Wiley) chapter 6 (Electron Spin-echo Studies of Relaxation Processes in Molecular Solids)
[28] Schweiger A and Jeschke G 2001 *Principles of Pulse Paramagnetic Resonance* (Oxford: Oxford University Press)
[29] Deligiannakis Y, Loulodi M and Hadjiliadis N 2000 *Coordination Chem. Rev.* **204** 1
[30] Reijerse E J, Shane J, de Boer E, Höfer P and Collison D 1991 *Electron Magnetic Resonance of Disordered Systems* ed N D Yordanov (Singapore: World Scientific) p 253
[31] Gramza M, Hilczer W, Goslar J and Hoffmann S K 1997 *Acta Chem. Scand.* **51** 57
[32] Hoffer P, Grupp A, Nebenfuhr H and Mehring M 1986 *Chem. Phys. Lett.* **132** 279
[33] Goldfarb D, Kofman V, Libman L, Shanzer A, Rahmatouline R, VanDoorslaer S and Schweiger A 1998 *J. Am. Chem. Soc.* **120** 7020
[34] Gemperle C, Aebli G, Schweiger A and Ernst R R 1990 *J. Magn. Reson.* **88** 241
[35] Dikanov S A, Tyryshkin A M and Bowman M K 2000 *J. Magn. Reson.* **144** 228
[36] Stoll St, Calle C, Mitrikas G and Schweiger A 2005 Advanced techniques and applications of EPR *38th Annual Int. Meeting of the ESR Group of RSC (Bath UK, March 2005)*

[37] Deligiannakis Y, Astrakas L, Kordas G and Smith R A 1998 *Phys. Rev.* B **58** 11420
[38] Krimse R, Kohler K, Abram U, Bottcher R, Golic L and de Boer E 1990 *Chem. Phys.* **143** 75
[39] Pointi A 1997 *J. Magn. Reson.* **127** 87
[40] Schwartz L J, Stillman A E and Freed J H 1982 *J. Chem. Phys.* **77** 5410
[41] Hoffmann S K, Goslar J, Hilczer W, Agustyniak-Jablokow M A and Kiczka S 2001 *J. Magn. Reson.* **153** 56
[42] Kasturi S R and Moran P R 1975 *Phys. Rev.* B **12** 1874
[43] Venkataraman G, Sahoo D and Balakrishnan V 1989 *Beyond the Crystalline State: An Emerging Perspective* (Berlin: Springer)
[44] Fischer K H and Hertz J A 1991 *Spin Glasses* (Cambridge: Cambridge University Press)